ELSEVIER

Astroparticle Physics 3 (1995) 231-238

Astroparticle Physics

The new Tien-Shan Atmospheric Čerenkov Telescope (TACT). Contemporary status: all-particle spectrum measured

R.A. Antonov [a], A.M. Anokhina [a], V.I. Galkin [a], E.E. Korosteleva [a], L.A. Kuzmichev [a], K.V. Mandritskaya [a], E.A. Petrova [a], T.M. Roganova [a], G.A. Samsonov [a], W. Tkaczyk [b]

[a] *Institute of Nuclear Physics, Moscow State University, 119899 Moscow, Russia*
[b] *University of Łódź, Pomorska 149 / 153, 90-236, Łódź, Poland*

Received 8 June 1994; revised 21 November 1994

Abstract

Results for the primary cosmic ray energy spectrum at 100–1000 TeV, data on the lateral distribution function for Čerenkov light of EAS and curvature of Čerenkov photon front are presented. Measurements were carried out using an array for observation of discrete gamma-sources in the TeV region.

1. Introduction

The Čerenkov method was first used for observation of extensive air showers (EAS) by Galbraith and Jelley [1]. Later it was developed for study of EAS characteristics in the energy ranges 10^{15}–10^{17} eV [2–4] and about 10^{13} eV [5]. The use of Čerenkov light for the search for discrete gamma-sources was began in 1960 by Chudakov et al. [6]. At present this method is used by different gamma-astronomical groups in the energy range 0.1–100 TeV (VHE gamma-astronomy).

The results of recent measurements at energies > 1 TeV do not confirm the existence of some gamma sources that were observed at these energies earlier. At the same time the existence of other sources (Crab, Mrk 421 AGN) is confirmed at a high level of confidence [7,8]. Therefore the main goals of VHE gamma-astronomy are to increase the experimental sensitivity for finding gamma-sources in the TeV region and to measure their energy spectra. Another important problem is the creation of the gamma telescope network that would be able to observe the gamma-sources intensity variation.

There exist two main modifications of the Čerenkov method. These are "image-sampling" and "time-sampling". The first one implies the using of the parabolic or spherical mirror directed accurately to the object that has some number of PMTs in the focal plane (for example Whipple [7], HEGRA [9], GT-48 in Crimea [10]). The pattern of light for each shower is analyzed to locate the EAS axis and to determine the primary particle type. The "time-sampling" technique presents an array of observation points that are also mirrors with PMTs (THEMISTOCLE [11], ASGAT [12]). One has to measure the arrival time and amplitude of the Čerenkov light at

SSDI 0927-6505(95)00002-X

each point to obtain the arrival direction and other characteristics of the primary particle. TACT array constructed in the Tien-Shan mountains belongs to this latter type of gamma-telescopes. For each event the location of the shower axis, the arrival direction of the primary particle and the energy of the particle are determined. This allows one to obtain the energy spectrum of the charged component of high energy cosmic rays in the range from a few TeV up to about 1000 TeV or even a few PeV as a "by-product" of gamma-astronomy. Such measurements are of interest in connection with some experimental evidence [13–15] for the possibility of a sharp steepening of the primary proton spectrum in the TeV region. It has to cause some feature in the all-particle spectrum. Modern experimental data are not rich enough to give conclusive results. It is necessary to carry out measurements in a wide energy range by the same device with high energy resolution. Detection of EAS Čerenkov light permits such an experiment, but it has not yet been carried out. Further measurements of the "knee" at $\sim 10^{15}$ eV are of great interest too.

2. Detector array

The detector array is situated in the Tien-Shan mountains at a height of 3300 m (43°04′11″ north latitude, 5 h 07 m 52.3 s east longitude) 40 km from Alma Ata (Kazakhstan). At present it consists of six parabolic mirrors, situated in the vertices of a regular hexagon, and a data collecting and processing center. The radius of the array is approximately 115 m. The mirror diameter is 1.5 m. In the focal surface of each mirror there is a photomultiplier. During the preliminary technical runs we used FEU-49B PMT (photocathode diameter 15 cm), which yields an angular aperture of about $6 \times 6°$. Photomultiplier signals were transmitted to the data processing centre through a coaxial cable 150 m long. Charge measurements were carried out using strobed (strobe duration 30 ns) 12-bit ADC. For timing purposes a constant fraction discriminator and 10-bit TDC with 0.6 ns time bin were used. 6-fold coincidence (within 0.6 μs gates) signal was used as a trigger

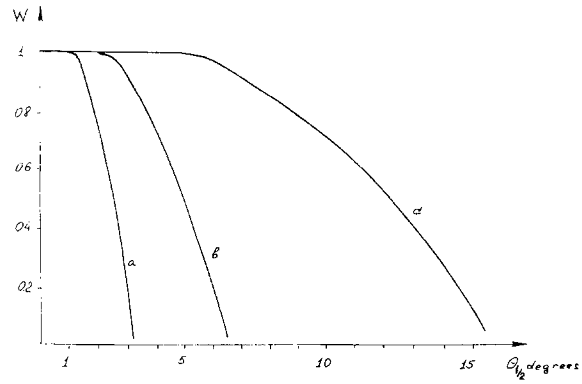

Fig. 1. Angular sensitivity of the detector versus detector cone half-angle $\theta_{1/2}$ for different diameters of photocathode. (a) 8 cm, (b) 15 cm (FEU-49), (c) 37 cm ("Quasar").

and start signal for TDCs. The array timer may be set by an external synchro signal.

The very important parameter of our array is the Čerenkov front timing accuracy for a single detector under heavy background light conditions. Calculations [16] showed that TACT may yield angular resolution 0.1–0.15° if timing accuracy (standard deviation) is ~ 1 ns. FEU-49 has poor temporal resolution: one-electron pulse jitter (FWHM) is ~ 20 ns wide which means it is impossible to achieve enough timing accuracy (and thus high angular resolution of the array) if the number of registered photoelectrons at each of six points is less than $\sim 10^3$. Later we plan to use the "Quasar" phototube, which is already used by the Baikal neutrino telescope NT-200 [17]. The "Quasar" phototube has good temporal characteristics (jitter < 3 ns) and large photocathode area (diameter is 37 cm). Angular aperture of the detector will amount to about $12 \times 12°$ while timing accuracy may be about 1 ns [17]. Fig. 1 shows the angular sensitivity W and Fig. 2 shows the area with $\sim 100\%$ efficiency of registration for FEU-49 and "Quasar".

3. Energy treshold

The energy threshold is determined by the ratio $U/\sigma(u)$ where U is the amplitude of the Čerenkov flare and $\sigma(u)$ is the standard deviation of the amplitude u determined by starlight background.

If the current pulse from the PMT is of the form

$$i(t) = i_0\, e^{-t/\tau_0}$$

and the output of the PMT has $\tau_1 = RC$ then we have

$$\sigma(u) = qR\sqrt{\frac{n}{2(\tau_1+\tau_0)}}$$

where n is the number of photoelectrons per second due to starlight, q is the output charge corresponding to one photoelectron. $\tau_0 \simeq 10^{-7}$ s for FEU-49.

If $\tau_1 \ll \tau_0$ then

$$\frac{U}{\sigma(u)} = \frac{Q}{q}\sqrt{\frac{2}{n\tau_0}}$$

where Q is the output charge due to a Čerenkov flare. To evaluate $n = I \cdot s \cdot \Omega \cdot k$ we used the following values: $I = 10^{12}$ photons/m^2 s sr – the starlight intensity, $s = 1.8$ m^2 – the area of mirror, $\Omega = 2.2 \times 10^{-2}$ sr – the effective detector solid angle, and $k = 0.04$ – the photocathode quantum efficiency and sum losses of light in the detector.

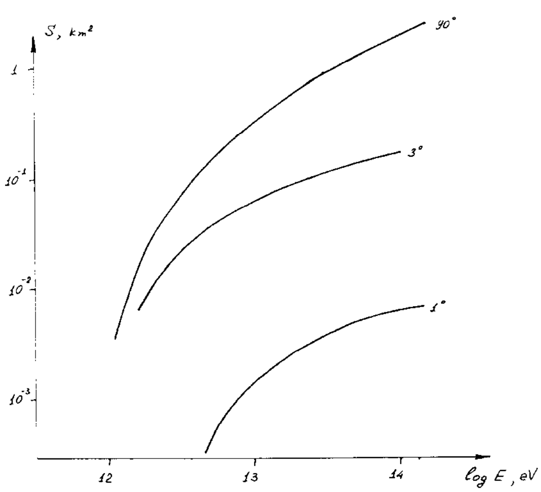

Fig. 2. Area of registration with 100% efficiency versus EAS energy for different PMT half-angles.

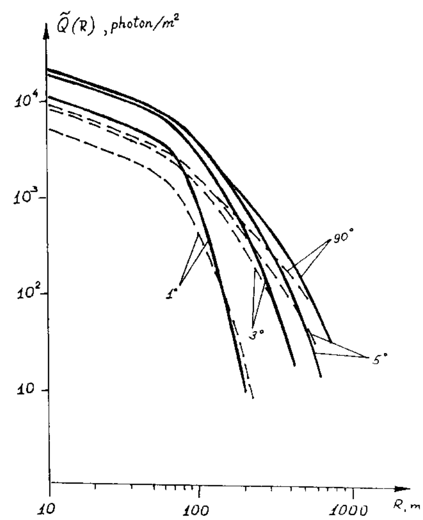

Fig. 3. Čerenkov light lateral distribution function for wavelength band 300–800 nm. Solid curves – primary gamma quanta; dashed curves – primary protons. $E = 10$ TeV. Half-angles are plotted in the figure.

If the trigger condition is $U/\sigma(u) > 5$, then the threshold signal at each detector is $U_{\text{thr}} \simeq 40$ photoelectrons. Such a threshold corresponds to the photon flux density 610 photons/m^2. The threshold energy is determined by the shape of the lateral distribution function (LDF). Fig. 3 shows LDFs calculated for TACT with different angular aperture (i.e. different PMTs). For FEU-49 with $\theta_{1/2} \simeq 3°$ the threshold energy for a primary gamma will be few TeV, while for protons ~ 10 TeV.

4. Rejection of charged particles background

The sensitivity of a ground-based gamma-telescope in a high background situation is determined by its angular resolution and the possibility of the flash image analysis. One way to improve the rejection is to record stereoscopic images of the Čerenkov flashes using two imaging telescopes [7,9]. Another way is the cooperation between the timing and the imaging gamma-telescopes which was suggested in Ref. [18]. Foreseeing this cooperation, the TACT array has been

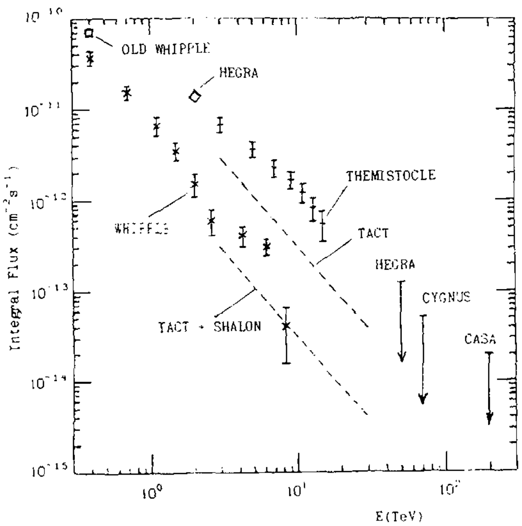

Fig. 4. Minimum detectable flux of gamma quanta for 30 h observation compared to data on the Crab [9].

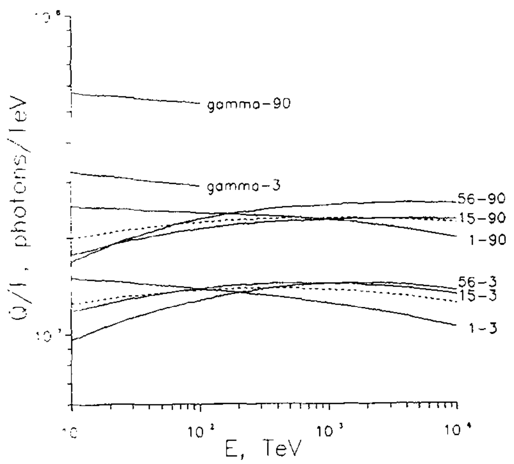

Fig. 5. Average total flux of the Čerenkov light in the 300-800 nm wavelength band for vertical showers. Observation level is 3200 m. Numbers by the curves are the masses of the primary nuclei and detector half-angles. Dashed curve corresponds to the charge composition from Ref. [23].

constructed around the SHALON imaging telescope [19]. The sensitivity in terms of the number of standard deviations above background can be expressed as

$$\frac{n_\gamma}{(2n)^{0.5}} = \frac{S_\gamma t F_\gamma f_\gamma}{(2St \cdot \pi\ \delta\theta^2\ Ff_{cr})^{0.5}}$$

where S_γ and S are registration areas for gamma-quanta and nuclei ($S_\gamma \simeq 2S$), t is time of exposure, F_γ, F are integral fluxes from point gamma-sources and nuclei. The factors f_γ and f_{cr} are the fractions of showers contributed after using of the selection criterion, where $\delta\theta$ is the telescope angular resolution.

Table 1 compares roughly the expected values of the main parameters of TACT and TACT + SHALON with the parameters of other telescopes.

Fig. 4 compares experimental data on Crab compiled in Ref. [20] with the evaluation of F_γ for TACT and TACT + SHALON. Here $f_{cr}^{0.5}/f_\gamma = 0.1$, $\delta\theta = 0.1°$, $t = 30$ h, $n_\gamma/(2n)^{0.5} = 3$, S_γ increases from 3×10^4 m^2 at 3×10^{12} eV to 10^5 m^2 at 3×10^{13} eV. The evaluation of $\delta\theta$ for TACT is derived from the Monte Carlo simulation [16].

5. EAS Čerenkov light as a measure of primary particle energy.

In order to clear up the question of EAS total Čerenkov light flux dependence on primary particle type, observation level and detector aperture a calculation was carried out. Fig. 5 shows the curves for the observation level 3.2 km for different primaries (proton, nuclei with $A = 15$, iron and gamma-quanta) and detector cones ($\theta_{1/2} = 3°$, 90°). The basic principles of the corresponding calculation are described in Ref. [21]. The hadron–hadron interaction model used in the

Table 1
The main parameters of gamma-telescopes

Telescope	Whipple [7]	ASGAT [12]	THEMIST. [11]	TACT	TACT + SHALON
s_γ (m^2)	3×10^4	3×10^4	3×10^4	3×10^4	3×10^4
$f_\gamma/f_{cr}^{0.5}$	10	1	1	1	10
$\delta\theta$ (deg)	1.25	0.7	0.1–0.15	0.1–0.15	0.1–0.15
$n_\gamma/(2n)^{0.5}$ (arb.units)	1	0.2	1	1	10

calculation was described in Ref. [22]. In the framework of the model, based on accelerator data, the inelastic cross-section is assumed to behave as

$$\sigma(\sqrt{s}) = \sigma_0\left[1 + 0.03\ \ln(\sqrt{s}/0.1\ \text{TeV})\right]$$

($\sqrt{s}$ is total center-mass energy) which is believed to be due to the multiplicity increase in the pionization region and the inelasticity coefficient rising with s. As one can see in Fig. 5, the total Čerenkov light flux at the TACT observation level is proportional to the primary energy in the 10–10^4 TeV region to within 10% accuracy on the assumption of invariable primary cosmic ray composition (see dots for $\theta_{1/2} = 3°$). In the 10^2–10^3 TeV region this statement holds for any possible behavior of primary composition from pure proton one to pure iron one. The dashed line in Fig. 5 corresponds to the composition measured in the SOKOL experiment at 10 TeV: 31% protons, 30% helium, 14% CNO, 13% Z = 10–20, 12% iron [23].

To check our calculations we compared our results for the sea level and the full detector angle with the Yakutsk experimental data presented in Ref. [24] (see Fig. 6). Both data sets were reduced to the 300–800 nm wavelength band. One can see that our data agree with the Yakutsk results to better than 10% accuracy.

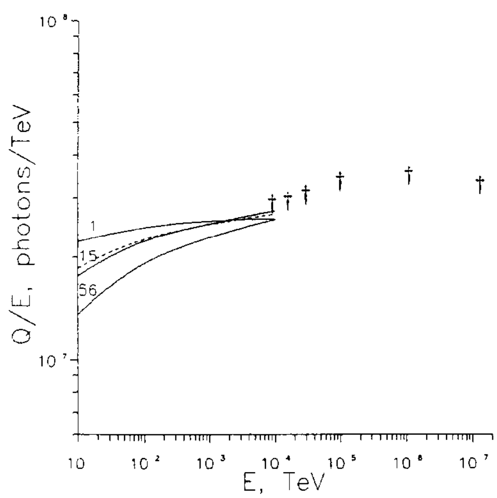

Fig. 6. Average total flux of the Čerenkov light in the 300–800 nm wavelength band for vertical showers observed by the full-angle detectors at sea level. Numbers by the curves are the masses of the primary nuclei. Crosses show the Yakutsk experimental data [24] for showers with zenith angles within 0–30°.

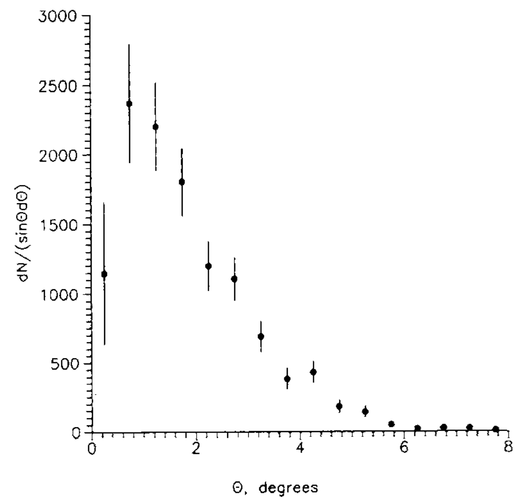

Fig. 7. Angular distribution of the detected showers.

6. Data analysis and results

In 1993 the first technical runs were carried out. All the detectors were aimed at the zenith with an accuracy of $\sim 0.1°$. Primary proton and nuclei background was measured under 6-fold coincidence. The threshold was about 270 photoelectrons. During 5.11×10^4 s 377 events were detected. Time stability of the detector and transparency of the atmosphere were monitored by the EAS counting rate.

Fig. 7 shows the angular distribution of the detected showers. The effective zenith angle of this distribution corresponds to the solid angle of array 9×10^{-3} sr. The data in Fig. 8 illustrate the spatial distribution of detected shower axes.

The data handling procedure includes three stages. First, the shower axis direction is estimated as an average of two directions, calculated using two independent threes of detectors under an assumption of a flat Čerenkov light front. Then, using amplitude data of all six detectors and transition coefficients "amplitude–photon number", shower core location and primary energy are calculated. At this stage the functional F_1 is minimized, which includes the pre-calculated dependence of the Čerenkov light LDF on primary energy [21]:

$$F_1 = \sum_{l=1}^{6} \frac{\left[Q_{i\,\exp} - Q_{i\,\mathrm{calc}}(E, x_0, y_0)\right]^2}{Q_{i\,\mathrm{calc}}^2}$$

where the Q_i are experimental and calculated numbers of photoelectrons at each of the six detectors, x_0 and y_0 are shower axis coordinates.

Finally, the arrival direction estimate has been improved. The procedure involves the fitting timing channel data to a pre-calculated light front model by minimizing of functional F_2:

$$F_2 = \sum_{i=1}^{6} \frac{\left[T_{i\,\exp} - T_{i\,\mathrm{calc}}(\theta, \varphi)\right]^2}{T_{i\,\mathrm{calc}}^2}$$

where the T_i are experimental and calculated arrival times for each detector, and θ and φ the shower axis direction.

To check the model of the shower Čerenkov image used by the handling procedure, at the first stage of the experiment special measurements were made of LDF and light front shape and the results were compared to the predictions. To exclude possible distortions due to the handling procedure itself, a special data bank was created of artificial events which were handled using the very same procedure as for experimental events. In the artificial sample shower axes were evenly spread over a circle of radius 400 m and energy was sampled from a power law (power index $\gamma = 1.6$). Fluctuations of photoelectrons were simulated as well as light front fluctuation in each detector. Total sample volume was 385 events.

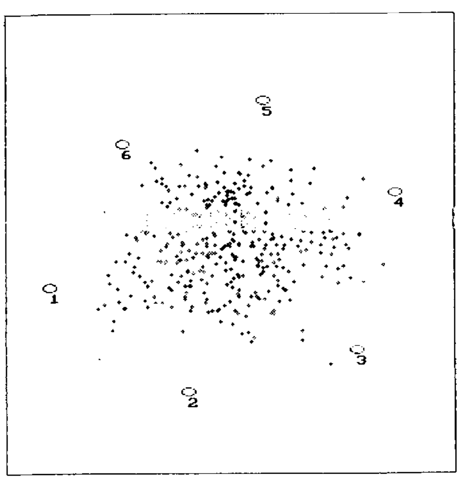

Fig. 8. Spatial distribution of the detected showers (top view).

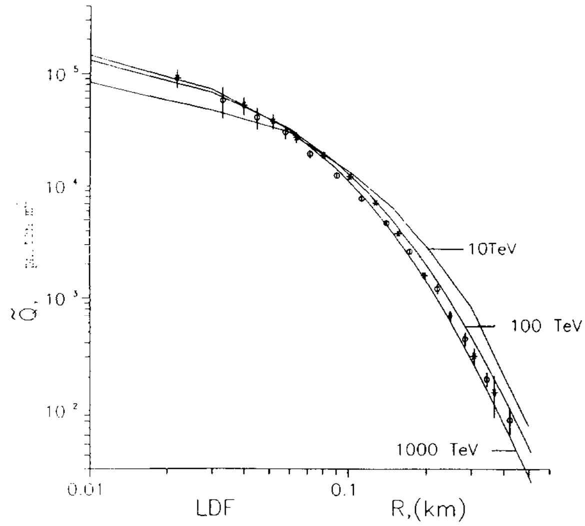

Fig. 9. Čerenkov light lateral distribution function. Solid curve – average LDF calculation, circles – experimental data, asterisks – simulated data.

Fig. 9 shows the calculated average LDF curves for $E_0 = 10$, 100, 1000 TeV and the results of experimental and simulated data handling. Simulations were carried out using a hybrid method [21] involving average calculation data shown. Experimental data were averaged over the whole energy range. It was assumed that the total amount of light was proportional to primary energy and that the shape of LDF is almost independent of primary energy. Numbers of photons, renormalized to 100 TeV under these assumptions, were combined in a curve. Calculated curves were normalized to 100 TeV in the same way. Comparison of experimental results with simulated data handling results and calculated curves shows good agreement. This proves that, on the one hand, the LDF shape is close to reality and, on the other hand, the handling procedure does not distort the LDF shape.

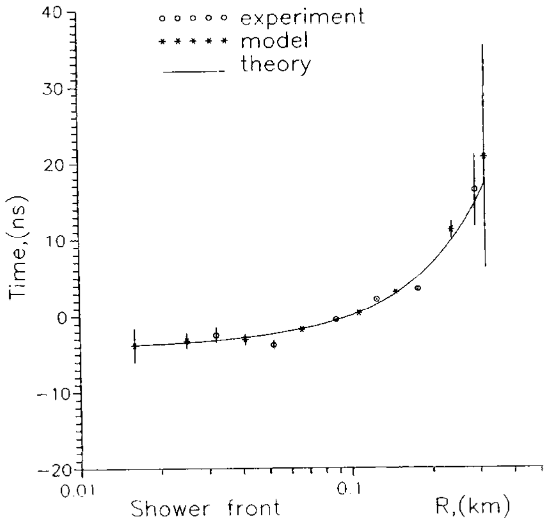

Fig. 10. Delay of the Čerenkov photon front versus the distance from the shower axis. Solid curve – average LDF calculation, circles – experimental data, asterisks – simulated data.

Fig. 10 shows the time delay of Čerenkov photons front versus the distance from the shower axis, also compared with artificial data handling

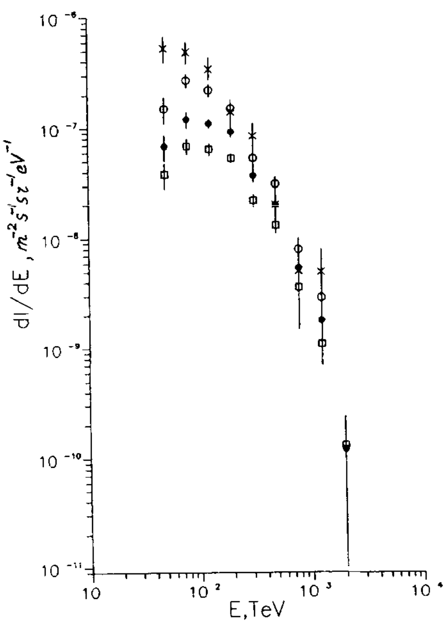

Fig. 11. Differential energy spectra for showers with axes within $R = 30$ m (asterisks), $R = 60$ m (open circles), $R = 90$ m (full circles), $R = 120$ m (squares).

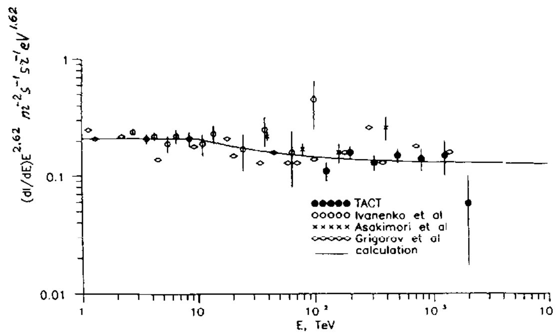

Fig. 12. All-particle differential energy spectrum.

results and calculated average curves. It was taken into account that within $\sim$ 90–110 m the fluctuations of photon front are minimal, the dependence on distance is weak and in almost all events there is at least one detector which has a distance from the axis 90–110 m. For this reason the time delay was calculated from the detector that was within the 90–110 m interval from the axis. The arriving time for this detector was considered as zero time. Using Fig. 10 one can draw the same conclusion as made while considering Fig. 9.

To obtain the undistorted spectrum of primary cosmic rays one has to use only events with parameters that yield practically 100% efficiency of registration. This criterion depends on the distance from the centre of array and on the primary particle energy. To evaluate the efficiency the differential spectra of events with axes within 30 m, 60 m, 90 m and 120 m from the array centre were analyzed (Fig. 11). For each of these radii there exists a threshold energy where the spectrum becomes a power law, and events that belong to the power spectrum (beginning from the biggest radius) were taken for the final processing. These were 213 events. Fig. 12 presents the differential energy "all-particle" spectrum as derived from our experiment compared with data of Refs. [14,25,26]. Spectral indices for 100–2000 TeV, 200–2000 TeV and 200–1500 TeV are 2.60 $\pm$ 0.11, 2.69 $\pm$ 0.12 and 2.64 $\pm$ 0.12 respectively (only statistical errors are indicated). We evaluate the systematic uncertainty of intensity connected with the energy measurement as 20–30%. The solid line is the illustration of the spectral feature that will take place if the proton spectral index is 0.6 more at 10 TeV. Much more experimental accuracy is needed to study such a feature than in previous experiments.

7. Conclusion

Test runs of the TACT array made it possible to test its ability to determine individual shower parameters as well as to measure the cosmic ray spectrum. The results obtained are consistent with theoretical calculations and with results of other authors. As to the energy spectrum of the charged component, the problem of possible proton spectrum steepening in the 1–100 TeV range may be solved by increasing the statistical accuracy and by measurement of the all-particle spectrum over this energy region with the same apparatus. TACT, having energy resolution about 30%, may try to solve this problem (no matter what primary composition would be as it was shown above) when its energy threshold will be decreased to a few TeV. From the other point of view it is possible to obtain data on the "knee" at $\sim 3 \times 10^{15}$ eV if the observation time will be long enough.

Acknowledgements

This work was partially supported by individual Soros Foundation Grants in Aid (R.A. Antonov, A.M. Anokhina, V.I. Galkin, G.A. Samsonov), the American Astronomical Society (R.A. Antonov) and Łódź University Grant UL 505.

Special thanks are due to professor S.I. Nikolsky for effective help.

References

[1] W. Galbraith, J.V. Jelley, Nature 171 (1953) 349.
[2] A.S. Krieger, H.V. Bradt. Phys. Rev. 185 (1969) 1629.
[3] M. Chantler et al., Proc. 16 ICRC, Kyoto 9 (1979) 42.
[4] A.A. Andam et al., Phys. Rev. D 26 (1982) 23.
[5] H. Tornabene, Proc. 16 ICRC, Kyoto 9 (1979) 94.
[6] A.E. Chudakov et al., J. Phys. Soc. Japan 17 Suppl. A 3 (1962) 106.
[7] P.T. Reynolds et al., Astrophys. J. 404 (1993) 206.
[8] G. Mohanty et al., Proc. 23 ICRC, Calgary 1 (1993) 440.
[9] F. Krennrich et al., Proc. 23 ICRC, Calgary 1 (1993) 251.
[10] B.M. Vladimirsky et al., Proc. of the Intern. Workshop on Very High Energy Gamma Ray Astronomy, Crimea, USSR (1989) 21.
[11] P. Bailon et al., Proc. 22 ICRC, Dublin 1 (1991) 220.
[12] V. Basiuk et al., Proc. 22 ICRC, Dublin 2 (1991) 231.
[13] V.I. Zatsepin et al., Yad. Fiz. 57 (1994), to be published (in Russian).
[14] K. Asakimori et al., Proc. 22 ICRC, Dublin 1 (1991) 57.
[15] N.L. Grigorov et al., Yad. Fiz. 11 (1970) 1058 (in Russian).
[16] R.A. Antonov et al., Proc. 22 ICRC, Dublin 2 (1991) 664.
[17] R.A. Antonov et al., Izv. Akad. Nauk 57 (1993) 181 (in Russian).
[18] R.A. Antonov et al., Voprosy Atomnoi Nauki i Techniki 4 (39) (1988) 47 (in Russian).
[19] R.A. Antonov et al., Preprint FIAN 172, Moscow, 1989 (in Russian).
[20] T.J. Haines, Proc. 23 ICRC, Calgary, Rapporteur Papers, (1993) 341.
[21] A.M. Anokhina et al., Astrophys. Space Sci. 209 (1993) 19.
[22] I.P. Ivanenko et al., Yad. Fiz. 29 (1979) 694 (in Russian).
[23] I.P. Ivanenko, et al., Proc. 23 ICRC, 2 (1993) 17.
[24] M.N. Dyakonov, et al., Izv. Akad. Nauk 57, (1993) 86 (in Russian).
[25] N.L. Grigorov, I.D. Rapoport, V.Ya. Shestoperov, High Energy Particles in Cosmic Rays (Nauka, Moscow, 1973).
[26] I.P. Ivanenko et al., JETP Lett. 49 (1989) 192.